Effect of Leading and Secondary Vortices on the Propulsion Performance of an Undulating Swimmer in the Periodic Vortex Street

Ruoxin Li[a,b], Pengfei Wang[a], Laibing Jia[c] , Yang Han[b,*] and Kai Yu[a]

a. Qingdao Innovation and Development Centre of Harbin Engineering University, Qingdao 266000, China

b. College of Shipbuilding Engineering, Harbin Engineering University, Harbin 15000, China

c. Department of Naval Architecture, Ocean and Marine Engineering, University of Strathclyde, Glasgow G4 0LZ, UK

(*Correspondence: hanyang@hrbeu.edu.cn)

Abstract

Aquatic animals have evolved diverse swimming techniques. They have demonstrated abilities to harness energy from vortices, particularly the Kármán vortex street, resulting in enhanced thrust. However, gaps remain in comprehensively understanding the factors influencing this increased thrust and the specific hydrodynamic characteristics involved. In this study, we studied an undulating foil downstream a circular cylinder to further understand the flow control mechanism involved in optimizing energy capture from hydrodynamic disturbances. We utilised numerical simulations with a moving adaptive mesh in laminar flow. We found that the leading vortex and secondary vortex at the foil's leading edge, originating from the Kármán vortex, played a crucial role in thrust enhancement. The undulating foil was more efficient in capturing energy from the Kármán vortex street than a stationary foil. When the foil was nearer to the cylinder, the energy capture was more evident, leading to intricate vortex patterns and easier leading vortex and secondary vortex generation.

This is a peer-reviewed, accepted author manuscript of the following article: Li, R., Wang, P., Jia, L., Han, Y., & Yu, K. (2024). Effect of leading and secondary vortices on the propulsion performance of an undulating swimmer in the periodic vortex street. Applied Ocean Research, 150, Article 104119. https://doi.org/10.1016/j.apor.2024.104119

The foil's lift initially rose with closer proximity but decreased with increased distance. Our results showed that for minimal drag and optimal lift, the cylindrical body's position is closely tied to the interaction between the Kármán vortex street and the undulating foil. These insights can be applied in applications of designing efficient propulsion systems for underwater vehicles and optimising energy harnessing mechanisms in marine environments.

Nomenclature

UI-SF	Uniform inflow-stationary foil
UI-UF	Uniform inflow-undulating foil
VS-SF	Vortex shedding-stationary foil
VS-UF	Vortex shedding-undulating foil
D	Diameter of cylinder
l	Longitudinal distance between the leading edge of the undulating foil and the centre of the cylinder
d	Lateral distance between the leading edge of the undulating foil and the centre of the cylinder
U	Velocity of the incoming flow
$h(x,t)$	Vertical excursion of the midline
$a(x)$	Undulating amplitude of the midline
x	Lengthwise coordinate measured from the tip of the fish nose
t	Time
λ	Wavelength
f_0	Undulating frequency of foil
f_e	Shedding frequency of vortex
T	Undulation period
A	Maximum undulating amplitude of the fish's midline

$\vec{u}$	Velocity vector
ρ	Fluid density
p	Pressure
μ	Dynamic viscosity
Re	Reynolds number
C_D, C_L, C_t	Drag, lift and thrust coefficient of foil
C_D^C, C_L^C	Drag and lift coefficient of cylinder
F_D, F_L	Drag and lift force of foil
F_D^C, F_L^C	Drag and lift force of cylinder
$\overline{C}_t$	Average thrust coefficient of foil
$\Delta\overline{C}_t$	Net thrust coefficient of foil
Δt	Time-step size

1.Introduction

Aquatic animals have evolved over millions of years to adapt to various marine environments. A notable aspect of their adaptations is the variety of swimming styles developed by these organisms. Manta rays exhibit gliding[1], while some other small fish display quick[2], darting motions, illustrating the diversity of swimming techniques in the marine world. Among these diverse swimmers, certain fish species stand out due to their unique physical characteristics that allow them to minimise the separation of boundary layers[3]. By reducing drag, these fish can move swiftly through water, expending less energy and thus having an evolutionary advantage in terms of survival and predation.

In recent decades, researchers have conducted in-depth studies on the fluid dynamics performance of fish[4][12] or schools of fish[13][18] in steady flows. However, in their natural habitats, fish often encounter obstacles such as rocks, corals, and human-

made structures. Instead of merely avoiding these obstacles, fish utilise the disturbances caused by the obstacles to their advantage. For instance, when encountering obstacles, many fish species prefer to position themselves downstream. This strategic positioning allows them to harness energy from the vortices formed behind these obstacles. The potential vortices in the ocean could thus become an energy source[19].

This behaviour of fish, especially their ability to harness energy from vortices, has been a subject of scientific curiosity for years. Early investigations into this phenomenon were pioneered by researchers like Liao et al.[20][21], who conducted experiments with rainbow trout. They simulated natural hydrodynamic disturbances by placing a stationary cylinder in front of a Rainbow trout. The trout exhibited a distinct swimming pattern when faced with these vortices. It synchronised its movements with the shedding vortices in a pattern named "Kármán gait". Their studies showed the trout was not just passively affected by the vortices but was actively harnessing energy from them. Beal et al.[22], in their experiments, reinforced these findings. They demonstrated that a flexible body, even without active control, can extract energy from the Kármán Street vortices. The extracted energy was sufficient to overcome the resistance and allow the flexible body to maintain its position and mov e upstream in the wake of a cylinder. Recent study by Harvey et al.[23] showed that a rainbow trout swimming in the wake of an oscillating hydrofoil can reduce its propulsion costs, even when swimming within the high-velocity zone of a vortex street.

Challenges arise in studying live fish behaviour due to unpredictability and the complexity of replicating oceanic vortex flows. Many researchers used numerical simulations to study fish behaviour. Liao et al.[24] used the two-dimensional Navier-Stokes equations to study a foil in a cylindrical wake. They found synchronisation between the vortex shedding frequencies of the foil and the cylinder. Eldredge and Pisani[25] simulated passive fish motion using three connected rigid bodies and found that certain fish was propelled upstream toward the cylinder whether the hinge was locked or not. Alben[26] modelled swimming in a vortex street, finding that optimal phase shifts between the body's trailing edge and the vortex for thrust and efficiency

vary with body size. Xiao et al.[27] found that a waving foil's thrust in a cylinder's wake increased across all tested gap ratios compared to a foil alone at the same frequency, but this increase diminished at higher frequencies and, for St values above 0.12, decreased with a greater gap ratios. Tong et al.[28] found linkage between lift and drag on the hydrofoil surface, which leads to nonlinear interactions, with their Immersed Boundary Boltzmann study on fish swimming in unsteady flows.

Researchers in bionic underwater robotics have closely followed these studies. Most current underwater robots, while impressive in their design, fail to replicate the intricate swimming abilities of real fish. They often mimic the shape and movement of aquatic organisms but fall short in replicating the fish's adaptive response to external changes, especially in vortex-rich environments. This deficiency underscores the importance of studying fish performance in vortex currents, not just for biological insights but also for advancements in underwater robotics.

Despite the wealth of studies and findings, gaps remain in our understanding of the phenomenon. While we know that fish can acquire energy and reduce locomotion costs in vortices, a systematic analysis of the reasons behind the increased thrust of fish in vortices is still elusive. Questions persist: Do stationary and undulating fish harness equal amounts of energy from vortices? What are the hydrodynamic factors that differentiate their performances? How does the position of the fish, especially the lateral distance from obstacles, influence their energy acquisition?

To address these questions and further our understanding, in this study we investigated the evolution of vortices when an undulating foil, representing a simplified fish model, was placed in a complex fluid field. Using a cylinder as a flow obstacle and providing an incoming flow at a specific velocity, we aim to simulate the conditions that generate vortices downstream of the obstacle. Through a series of models and simulations, we aim to understand the interaction between fish and vortices.

The subsequent sections of this paper are organised as follows. Section 2 provides details on the computational schemes, including the numerical methods used, the kinematic model of undulating fish, and the relevant parameters associated with the

problem studied. In Section 3, four types of models are conducted as summarised in Table 1: uniform inflow-stationary foil (UI-SF), uniform inflow-undulating foil (UI-UF), vortex shedding-stationary foil (VS-SF), and vortex shedding-undulating foil (VS-UF). These models aim to elucidate the underlying reasons behind the enhanced thrust generated by undulating foils by analysing the evolution of vortices. Additionally, a comparison is made regarding the differences in thrust performance of undulating foils at different lateral distances. Lastly, the analysis is extended to multiple locations, and the interaction effects between the cylinder and undulating foils are summarised.

2.Numerical models and methods

2.1 Problem Description

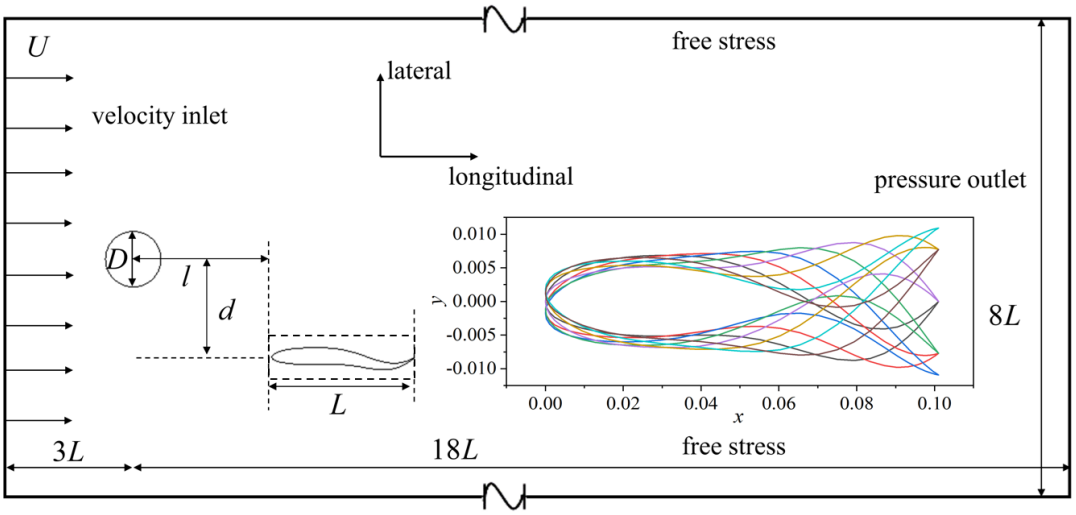

Figure 1 Sketch of computational domain

A schematic diagram of the two-dimensional physical model is shown in Figure 1. The setting of the computational domain is based on previous work[29]. A cylindrical section with diameter D is fixed in the midline. A NACA0012 foil[9] with a length of L undulates behind the cylinder. Here we define l as the longitudinal distance between the leading edge of the undulating foil and the centre of the cylinder, while d is their lateral distance. Both l and d can be adjusted. A uniform incoming flow with a velocity U is given at the inlet boundary. The up and bottom boundaries of the domain are set as

stress free, and the right boundary is set as pressure outlet.

The cross section of a fish body can be simplified into a NACA foil. This study uses a two-dimensional computational model to simulate the undulatory motion of fish. The undulating motion of the foil body can be seen in Figure 1. The deformation amplitude of the undulating foil is consistent with its midline. The undulating motion on the midline of foil in the present study follows a classical subcarangiform swimming from previous research[27][30][32] as

$$h(x,t) = a(x)\sin(2\pi(\frac{x}{\lambda} - f_0 t)) \tag{1}$$

Where $h(x,t)$ is the vertical excursion of the midline at a given time, $a(x)$ represents the midline's undulating amplitude, x is the lengthwise coordinate measured from the tip of the fish nose, and t is the time. λ denotes the wavelength, and f_0 is the undulation frequency. T is the undulation period, and it holds that $T = 1/f_0$. The amplitude $a(x)$ is expressed as a sinusoidal equation, following:

$$a(x) = A[0.351\sin(\frac{x}{L} - 1.796) + 0.359] \tag{2}$$

where A is the maximum undulating amplitude of the fish's midline.

2.2. Numerical scheme

Our study considered a one-way coupled fluid structure interaction problem, and it is solved using a commercial solver ANSYS-Fluent v16.2 with its UDF function defining the motion of the foil. The two-dimensional incompressible N-S equation is discretized by the finite volume method, and the equation is as follows:

$$\nabla \cdot \vec{u} = 0 \tag{3}$$

$$\frac{\partial \vec{u}}{\partial t} + (\vec{u} \cdot \nabla)\vec{u} = -\frac{1}{\rho}\nabla p + \frac{\mu}{\rho}\nabla^2 \vec{u} \tag{4}$$

where $\vec{u}$ is velocity vector, ρ is fluid density, p is pressure, μ is dynamic

viscosity.

A second-order upwind scheme is used for convective terms and the diffusion term is discretised with the second-order central-differencing scheme. Pressure–velocity coupling is achieved using the SIMPLE algorithm. Since the Reynolds number corresponding to fish swimming is generally low, the laminar flow model is used.

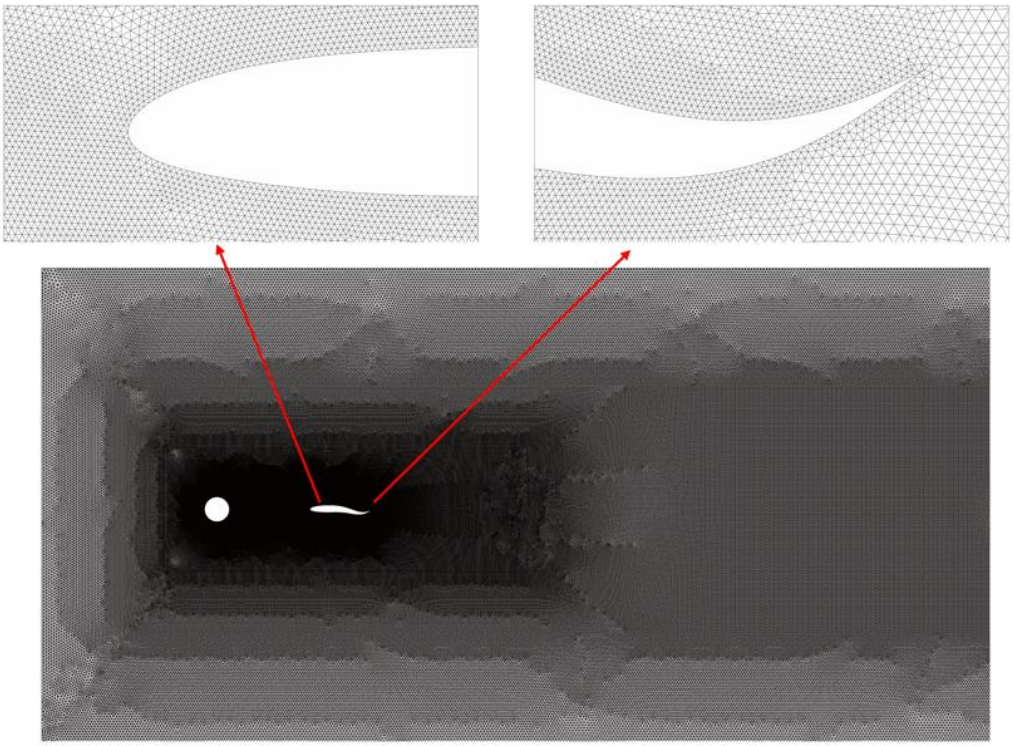

Figure 2 Sketch of mesh

The commonly used methods, such as immersed boundary method[33], overset method[31], smoothed particle hydrodynamics method[34][35] and remeshing method[27], can solve the problem of large deformation of fish models. Present study uses remeshing method to deal with the grid deformation problem around the bionic fish. The whole computational domain is discretised with unstructured triangular mesh as shown in Figure 2. The mesh becomes denser as it approaches the cylinder and foil. The surface of the foil should have over 500 body-fitted grid nodes to ensure accurate results.

2.3 Performance parameters

In our study, the Reynolds number (Re) is defined as:

$$Re = \rho UD / \mu \tag{5}$$

where ρ is fluid density, U is the velocity of the incoming flow, D is the diameter of the cylinder and μ is dynamic viscosity. The Strouhal number is defined as,

$$St = f_0 A / U \tag{6}$$

where f and A stands for the undulating frequency and amplitude of the foil, respectively.

To characterize the hydrodynamic performance of the undulating foil and cylinder, the drag and lift coefficients are defined as,

$$C_D = \frac{F_D}{\frac{1}{2}\rho U^2 L} \tag{7}$$

$$C_L = \frac{F_L}{\frac{1}{2}\rho U^2 L} \tag{8}$$

where F_D and F_L are obtained through integrating pressure and shear stress over the surface of the foil. The thrust is quantified with the thrust coefficient $C_t = -C_d$. Similarly, the drag and lift coefficients of the cylinder is determined by:

$$C_D^c = \frac{F_D^c}{\frac{1}{2}\rho U^2 D} \tag{9}$$

$$C_L^c = \frac{F_L^c}{\frac{1}{2}\rho U^2 D} \tag{10}$$

The average thrust coefficient $\overline{C}_t$ is used to evaluate the propulsion performance of the foil and written by:

$$\bar{C}_t = \frac{1}{T}\int_0^T C_t dt \tag{11}$$

A net thrust coefficient $\Delta\bar{C}_t$ is used in the present study to evaluate the performance improvement of the foil in the vortex field, and it is defined as the difference between the mean thrust coefficient of the other foil and that of a stationary foil which is placed in a uniform inflow (UI-SF) as,

$$\Delta\bar{C}_t = \bar{C}_t(other) - \bar{C}_t(SF) \tag{12}$$

2.4 Numerical validations

To validate the independence of the numerical results on the mesh density and time-step size, we carried out a series of simulations using a single foil with the undulating motion. In all the simulations, the length of fish L and wavelength λ are specified and fixed at λ L 0.1m. The maximum undulating amplitude is fixed at $A = 0.1L$. Three different time-step sizes are selected for time independence tests, where $\Delta t = 1/200T, 1/400T$ and $\Delta t = 1/800T$. The undulating period T is fixed at $T = 2s$. According to Figure 3(a), results are almost identical between $\Delta t = 1/400T$ and $\Delta t = 1/800T$, and a slight difference exists for $\Delta t = 1/200T$. Specifically, the maximum error between the minimum and the intermediate time step is 0.67%, and that between the maximum and the intermediate time step is 3.47%. Considering the accuracy and computational time, a time-step size $\Delta t = 1/400T$ is selected in the rest of our study.

Grid independence tests were conducted with a total number of 3.67×10^5 for coarse mesh, 5.21×10^5 for medium mesh and 9.24×10^5 for fine mesh, respectively. Computational results, as shown in Figure 3(b), the maximum error between the medium mesh and the coarse mesh is 2.73%, and the that between the medium mesh and the fine mesh is 0.85%. The difference in results between medium and fine mesh is minor. Therefore, medium mesh is adopted for all following simulations.

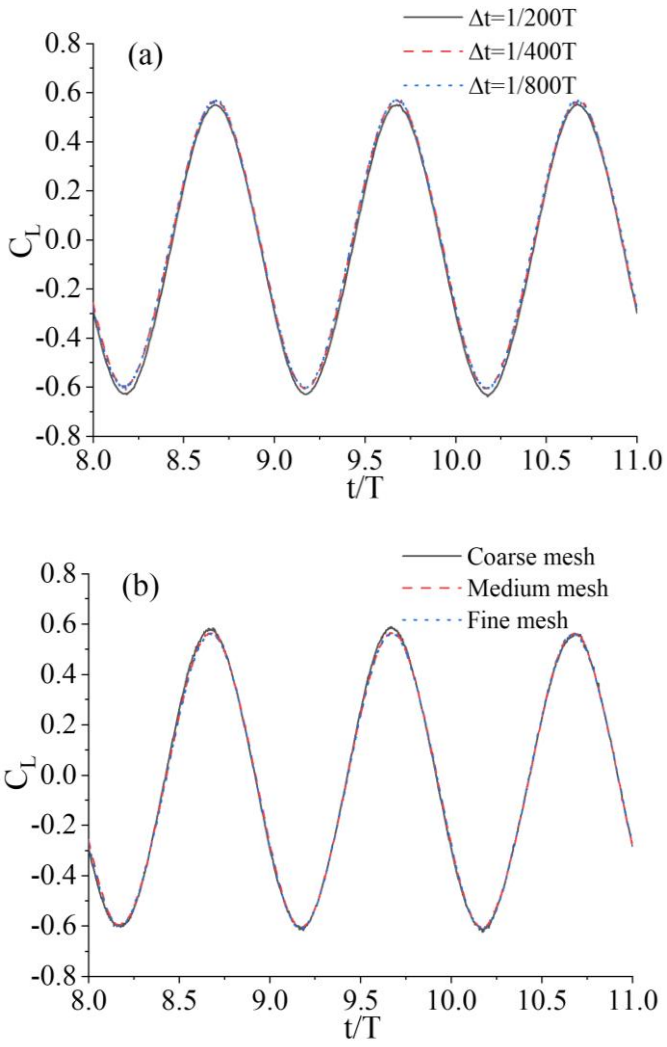

Figure 3 Independence tests (a) Different time-step sizes (b) Different Grid density tests.

In order to validate the numerical method presented in this work, a test case was compared with the work of Dong and Lu[36]. The flow over an undulating foil at $Re = 5000$ is computed, and the kinematics of the foil are described by Eq.1. The validation case was calculated using the converged mesh and converged time step. The time histories of the drag and lift coefficient during one time cycle are shown in Figure 4. Compared to the work of Dong and Lu[36], the differences of present simulation on the max drag and lift coefficients are 1.25% and 0.56%, respectively. The good agreement with previous results exhibited the numerical method employed in the present study is capable of simulating for fish-like swimming under unsteady flow

condition.

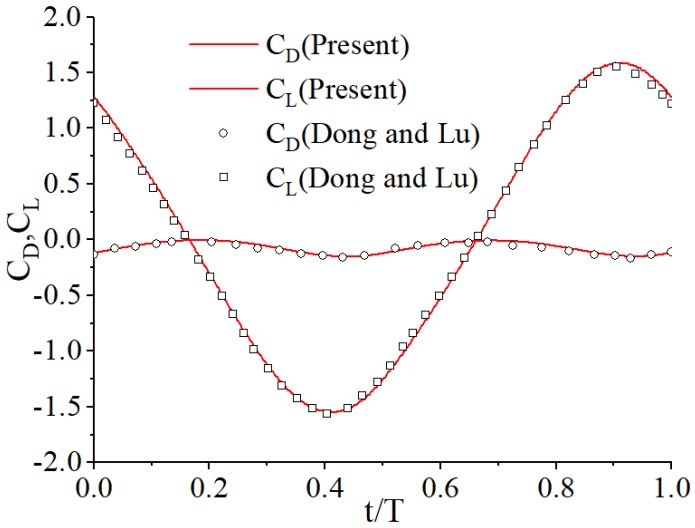

Figure 4 Comparison of the force coefficients within one time cycle for the undulating foil.

Table 1 Case Conditions

No.	Case Name	Cylinder	Foil	Flow Velocity
1	UI-SF	×	Stationary	✓
2	UI-UF	×	Undulating	✓
3	VS-SF	✓	Stationary	✓
4	VS-UF	✓	Undulating	✓

3.Results and Discussions

The hydrodynamic behaviour is initially examined across four distinct states, as outlined in Table 1. The parameters in all subsequent cases are given in Table 2. This analysis aims to illustrate the foil's performance under both uniform inflow and vortex street conditions. Subsequently, the study will focus on the performance of the undulating foil at varying lateral distances from a cylinder, with the lateral distance d/L varying between -1 and 1. Finally, we will investigate the performance of the undulating foil situated behind the cylinder, taking into account different translational and lateral distances. For these simulations, the longitudinal distance l/L will range

from 0.5 to 3, and the lateral distance d/L will range from -1 to 0.

Table 2 Parameters for all cases in present study

Parameter	Value
Cylinder Diameter D	0.04m
Undulating Period T	2s
Incoming Flow Velocity U	0.04m/s
Strouhal Number St	1.25
Reynolds Number Re	1600

3.1 Hydrodynamic Mechanisms of the Foil in Different Flow Conditions

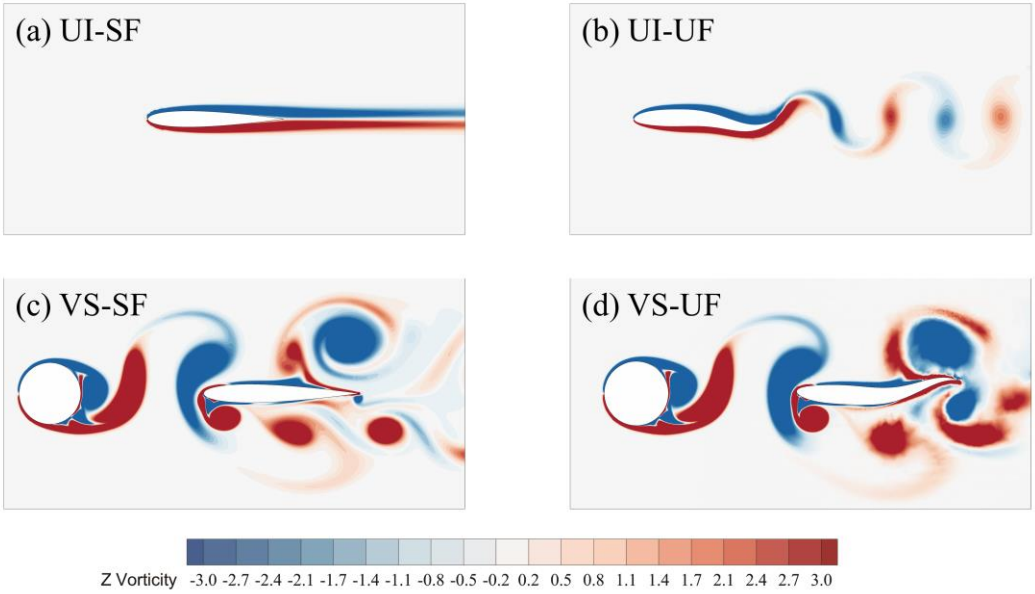

Figure 5 Vorticity contours of four cases: (a) the UI-SF case, (b) the UI-UF case, (c) the VS-SF case, (d) the VS-UF case.

Figure 5 displays the simulated results for four different cases. Among them, in both VS-SF and VS-UF case, the longitudinal distance between the foil and the cylinder is l/L 1 .0. Generally, when the foil is placed in a uniformed inflow, the upper surface of the foil is covered with a layer of negative vortex, while the lower surface is covered with a layer of positive vortex, as shown in Figure 5(a). The UF can generate pairs of

trailing vortices (Figure 5 (b)), compared with SF. When the shed vortices pass by the foil, interactions exist between the foil and positive or negative vortices. The formation and distribution of the vortices for those cases under VS condition are more complex. As presented in Figure 5(c) and (d), the Kármán vortex street sequentially passes and is split by the leading edge of the stationary or undulating foil.

Figure 6 shows the evolution of the dimensionless thrust for the four cases. As the incoming flow velocity is not zero in UI-SF, the thrust of the foil is negative. It was noted that the thrust of VS-UF is not a mere superposition of the values for VS-SF and UI-UF but is much greater than their sum. The mean thrust coefficient for the four cases are listed in Table 3. Due to the undulating motion, the foil experiences a fluid recoil force and gains a forward thrust. The net thrust of the UF is greater than that of the SF for both UI and VS conditions. For SF and UF in the VS conditions, the net thrust of the foil is much greater than that in the uniform inflow. Meanwhile, the net thrust difference between VS-UF and VS-SF is larger than that between UF and SF in the uniform inflow condition. In Table 3, results reveal that the net thrust of VS-UF is 53.3% more than the total net thrust of VS-SF and UI-UF. According to the results, an undulating foil is able to obtain a larger net thrust than a stationary foil, and the extra net thrust is not solely attributed to the undulation of the foil.

Table 3 Mean value and net thrust coefficient for each case

Case	l/L	$\overline{C}_t$	$\Delta\overline{C}_t$
UI-SF	-	-0.06012	0
UI-UF	-	-0.04005	0.02007
VS-SF	1.0	0.08840	0.14852
VS-UF	1.0	0.19861	0.25872

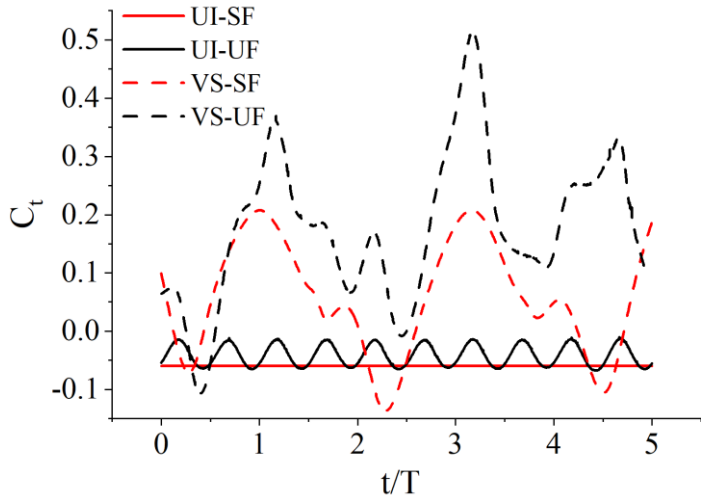

Figure 6 The evolution of thrust coefficient on foil within 5 sequential periods for four states

Upon analysing the vortex field, it becomes evident that the presence of a leading-edge vortex and a secondary vortex on the foil surface in the VS condition significantly contributes to the increased thrust, compared to the UI condition. Both negative and positive vortices can affect the vortex sequence arrangement on the foil surface. For the vortex field in Figure 7, a new leading-edge vortex L1 or L2 is generated by the vortex in the opposite direction on both upper and lower surfaces of the foil, respectively. Streamlines are presented in Figure 7(a) to illustrate the process of the negative vortex divided by the foil leading edge. A large angle is formed between the streamline and the centreline of the foil. There is an obvious flow separation below the edge, resulting in a leading-edge vortex L1 in the opposite direction.

Furthermore, a secondary vortex S1 forms between L1 and the surface of the foil. This secondary vortex is negative, and its existence weakens the original vortex distribution on the foil surface. In Figure 7(c), the secondary vortex creates areas with fast speed and the resulting low-pressure areas create suction on the surface of the foil. This phenomenon is similar to the formation of leading-edge vortex and secondary vortex produced by a pitching and plunging plate in a previous study[37]. The results indicate that a plate with a significant and effective attack angle in the incoming flow is capable of generating a secondary vortex. Concurrently, the leading-edge vortex undergoes a temporal evolution, marked by its initial formation, subsequent

concentration, and eventual separation from the shear layer. A comparable secondary vortex is also likely to manifest in following fish within schools[38][40]. Consequently, the phenomenon that both leading-edge vortex and secondary vortex can be found in the VS condition is probably due to the attack angle between foil and incoming flow, and the attack angle changes with time.

Whether the leading-edge vortex could separate from the foil also depends on the development of the Kármán vortex. As seen in Figure 7(b) and (d), when the foil passes through the positive vortex, a similar leading-edge vortex L2 and secondary vortex S2 are generated on the upper surface of the foil. At the same time, the upper surface of the foil has a high-pressure area and a suction area which enhance the thrust of the foil. This result is similar to the study of Joshi et al[41].

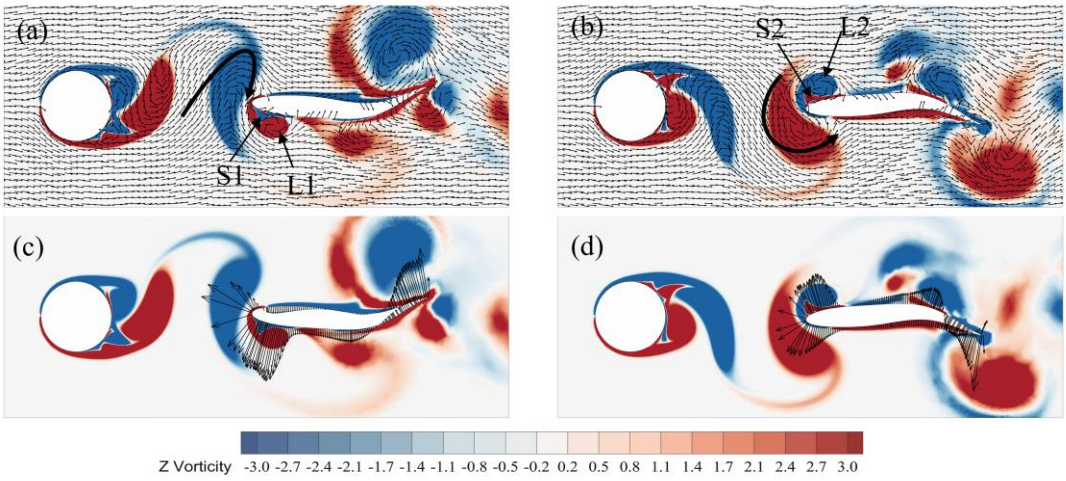

Figure 7 Positive and negative vortices pass the leading edge of the undulating foil in the VS-UF case. (a): velocity vectors corresponding to negative vortex. (b): velocity vectors corresponding to positive vortex. (c): When the negative vortex acts on the leading edge of the foil, the pressure distribution on the foil surface. (d): When the positive vortex acts on the leading edge of the foil, the pressure distribution on the foil surface.

During the evolution of the leading-edge vortex and secondary vortex, it was noted that the instantaneous force on the foil can be obviously affected. Results at several corresponding instants of the VS-UF case, i.e., time (a), (b), (c), and (d) marked in

Figure 8, is further discussed by combining with Figure 9.

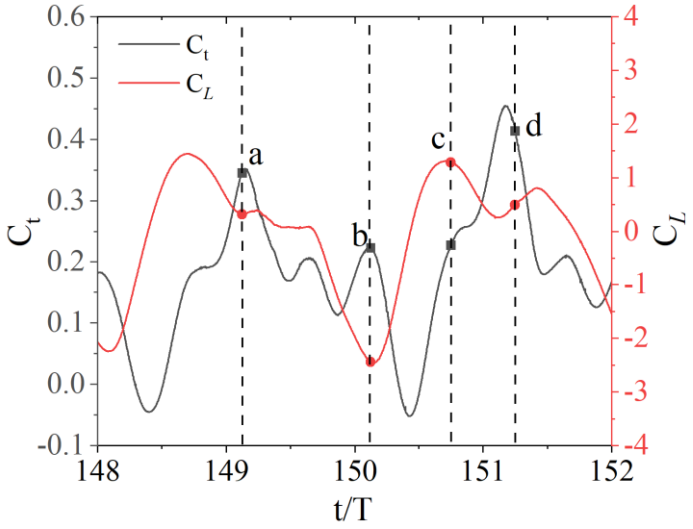

Figure 8 Thrust coefficient C_t and lift coefficient C_L of the foil within four time periods in the VS-UF case. We set l/L 1 , d/L 0 , Re 1 600 and f_0 0 .5hz.

Specifically at time a, the thrust on the foil reaches a peak value in Figure 8. The vortex passes through the undulating foil, and the leading-edge vortex L1 and secondary vortex S1 are generated.

At time b, P1 passes by the foil and is split into upper and lower parts, as marked in Figure 9(b). As shown in Figure 8, the thrust force of the foil reaches its peak value, and the absolute value of lift also achieves its maximum. Meanwhile, positive vortices acting on the leading edge of the foil are found to enhance the lift force as well when the suction region is at the upper edge of the foil. The negative vortex N1 passes through the leading edge of the foil. Considering the effects of the leading-edge vortex L2 and the secondary vortex S2, the thrust of the foil increases, and the direction of the lift is changed to downward. The secondary vortex S1 sheds off the surface of the foil, merges with the upper half of P1, and surrounds L1. The lower part of P1 promotes and controls the generation of S2 together with L2.

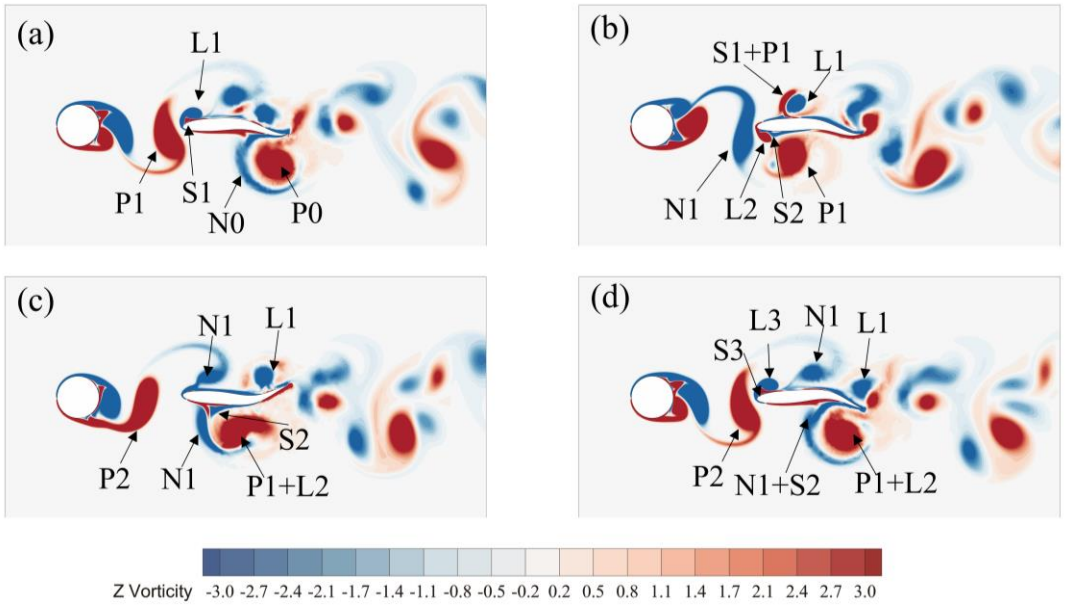

Figure 9 The evolution of the vortices for VS-UF case at moment a, b, c and d.

At time c, the leading vortex L2 gradually separates from the foil surface and merges with the forward vortex P1 and L1 moves to the trailing edge of the foil in Figure 9(c). And the force enhancement area is mainly concentrated on the trailing edge. Thus, the thrust increases at this moment.

With the fluid field changing with time, S2 weakens and merges with N1 at time d. At this point, there are three types of negative vortices above the foil, i.e., two leading edge vortices (L1, L3) and a divided Kármán vortex(N1) as shown in Figure 9(d). L1 merges with the trailing vortex generated by the undulation of the foil and discharges backwards. The Kármán vortex has the same effect on the foil over a long-time span, and the secondary vortex on the upper and lower surfaces of the foil may be separated, but the suction zone produced by the secondary vortex is very obvious. It was pointed out that the secondary vortex acts sequentially on the upper and lower surfaces of the foil to enhance the thrust and balance the lift force. However, the floating range of the lift force is very large, which greatly increases the instability of the foil.

The leading-edge vortex and the secondary vortex can also be found in the VS-SF case. Figure 10 compares the vorticity field when the leading-edge vortex moves to the trailing edge of the foil between the VS-UF and VS-SF cases. In area A and B, it was found that the secondary vortex can still generate a large suction force on the foil at the

trailing edge in the VS-UF case. Compared with B, the leading-edge vortex and secondary vortex in area A are significantly weakened. The suction area in A still exists but is small. The undulation of the foil leads to a large displacement of the trailing edge. Moving boundaries do not weaken the intensity of the secondary vortex. It is more conducive to the undulation of the foil and increases its thrust when the trailing edge displacement direction is consistent with the force direction. By combining the undulation of the foil with the suction provided by the secondary vortex, the thrust of the undulating foil is much greater than that of the stationary foil. This explains the phenomenon that the thrust of the VS-UF case is greater than that of the sum of VS-SF and UI-UF case.

The above discussions reveal that the generation of the leading-edge vortex and the secondary vortex is the reason for the enhancement of thrust of the undulating foil in the Kármán vortex street. Making full use of the energy of the secondary vortex is an effective way to improve the hydrodynamic performance of the undulating foil. Some vital factors, such as the relative position between the foil and the cylinder, the state of the undulation, can directly affect the absorption of the vortex energy by the foil.

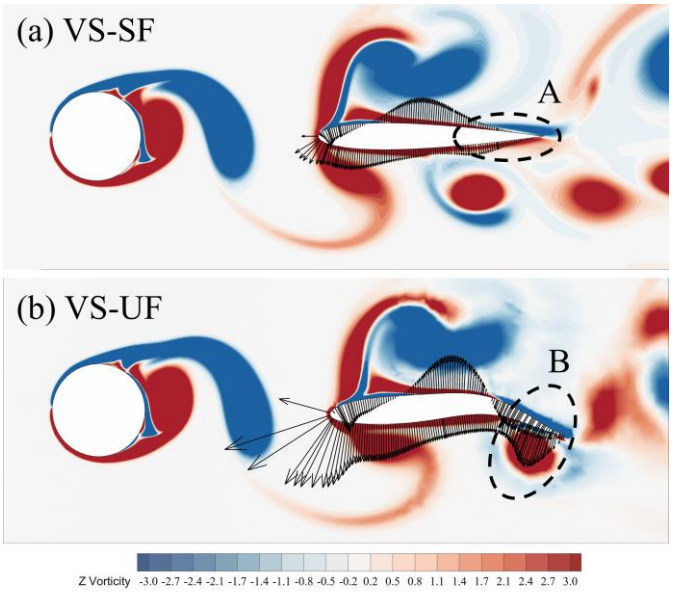

Figure 10 Vorticity contours when the leading-edge vortex moves to the trailing edge of the foil and the pressure vector line on the foil surface. (a): The VS-SF case. (b): The VS-UF case.

3.2 The Effect of Lateral Distance

Previous study[27] has demonstrated that the hydrodynamic performance of an undulating foil in the Kármán vortex street varied when longitudinal distance changed. However, the relation between the distribution of vortices, especially leading-edge vortex and secondary vortex, and the undulation foil with different lateral distances is still unknown. Thus, present section will carry out deep investigations on the hydrodynamic performance of an undulating foil in the Kármán vortex street with different lateral distances away from the cylinder. In this section, the longitudinal distance between the undulating foil and the cylinder is set to l/L 1.0.

Both $\overline{C}_t$ of the undulating foil and $\overline{C}_D^c$ of the cylinder with different lateral distances are shown in Figure 11 (a). As the foil undulates with the same manner for all the cases, the thrust coefficient can directly reflect its kinematic performance. The results indicate that the magnitude of the thrust is almost the same for the undulating foil at the symmetrical position about the centreline of the cylinder. There is no obvious change in thrust when the absolute value of d/L exceeds 0.7. When the absolute value of d/L is less than 0.4, the thrust coefficient of the foil increases significantly. Another finding is that within a certain range of lateral distance, the thrust of the foil increases dramatically first and then decreases. At d/L 0, the thrust reaches its peak value, which means that foil has achieved its best performance.

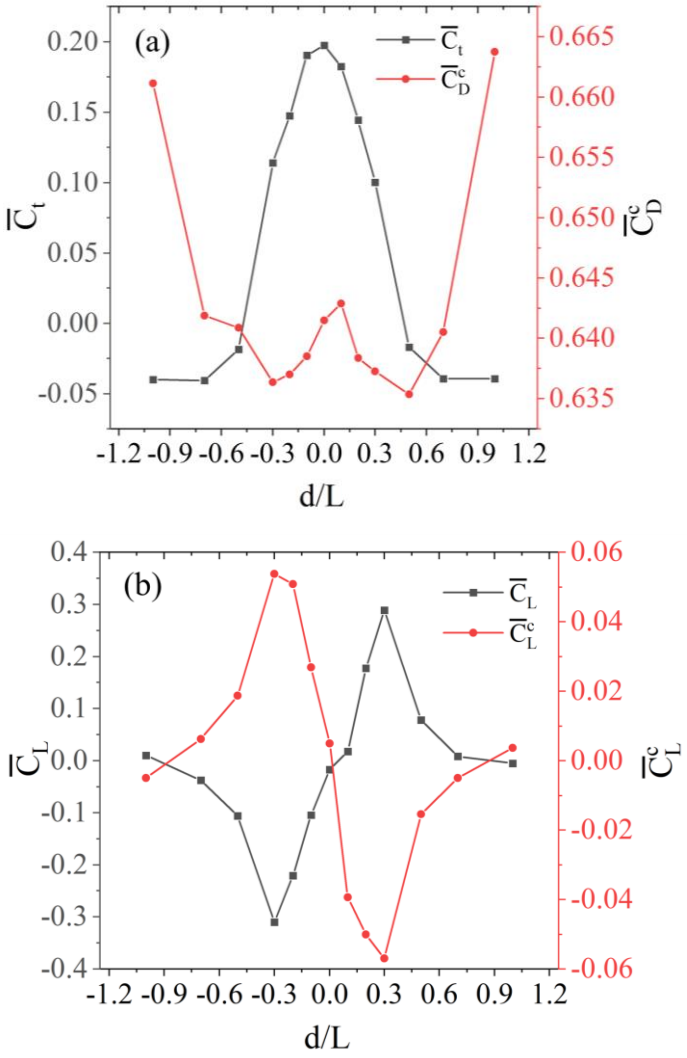

Figure 11 (a) The mean values of the thrust coefficient $\overline{C}_t$ of the undulating foil and drag coefficient $\overline{C}_D^c$ of the cylinder at different lateral distances. (b)The mean values of the lift coefficient of the undulating foil $\overline{C}_L$ and cylinder $\overline{C}_L^c$ at different lateral distances.

Furthermore, the results show that the foil swimming downstream reduces the drag of the cylinder obviously. The force acting on the cylinder and the foil in the *x* direction should be a pair of interaction forces, but their laws of change are different. In contrast to the thrust of foil, cylindrical drag decreases most when the absolute value of *d/L* is around 0.4. When the lateral distance decreases, the drag coefficient of the cylinder first decreases and then increases. There is no monotonous decrease in drag of the cylinder along with the decrease in the lateral distance.

The mean value of lift coefficients for the undulating foil and the cylinder with

different lateral distances are shown in Figure 11(b). When the foil is at the symmetrical positions about the centreline of the cylinder, the lifting forces has the same value but with an opposite direction. The lift coefficient presents the tendency of increasing first and then decreasing with the distance from the cylinder centreline decreasing. When *d/L* is around 0.3, the lift coefficient reaches its maximum. At *d/L* 0, the lift coefficient is almost zero. In contrast to the force in the *x* direction, a pair of interactions force acting in the *y* direction have the same variation trend. The lift force of the cylinder and foil develops in opposite directions.

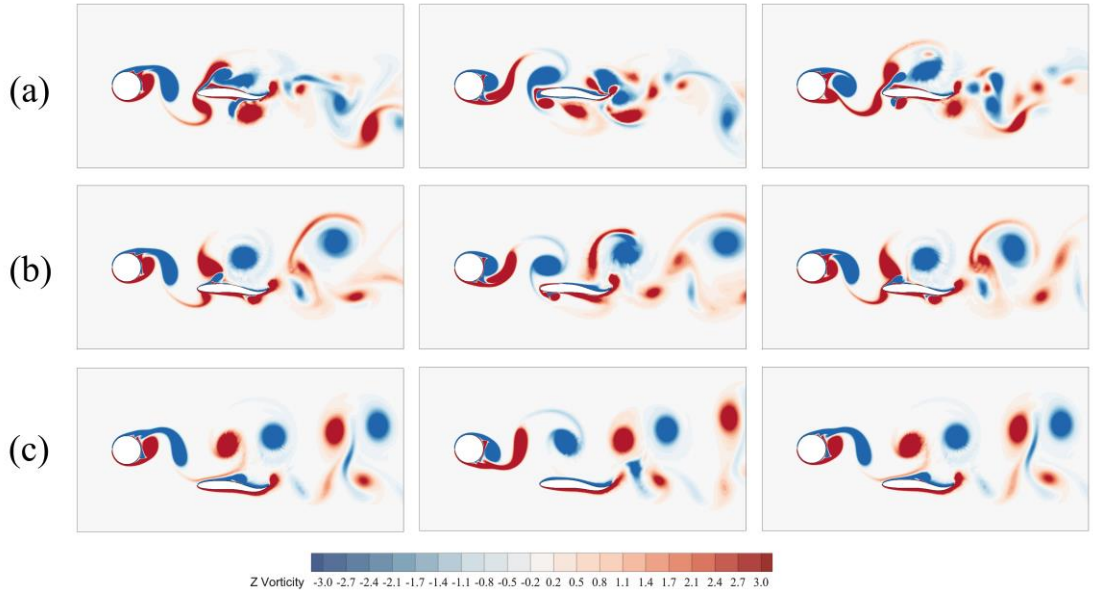

Figure 12 The vorticity contours of the undulating foil at different lateral distances below the cylinder.

(a) *d/L* -0.1, (b) *d/L* -0.3, (c) *d/L* -0.5. We set *l/L* 1 .0, *Re* 1 600 and f_0 0 .5Hz.

The vorticity contours of the undulating foil at different lateral distances from the cylinder are shown in Figure 12. The evolution of vortices is similar for cases with the same lateral distance on both the upper and lower sides of the centreline. This figure only displays the evolution and distribution of vortices on the lower side. When $d/L=-0.1$, the evolution law of the vortex is similar to that described above when *d/L* 0. When *d/L* -0.3, only a small part of the Kármán vortex is divided by the foil. The leading-edge vortex induced by the forward vortex on the upper surface of the foil separates from the surface earlier. In the case of *d/L* -0.3, the secondary vortex induced by the negative vortex experienced earlier separation. Due to the premature separation

of the leading-edge vortex on one side of the foil and the decrease in the intensity of the secondary vortex generated by the leading-edge vortex, the thrust of the foil is reduced compared to d/L 0.

The strength of the Kármán vortex on the upper and lower surfaces of the foil is also different. Coupled with the asymmetry of the secondary vortex, the lift of the foil cannot be balanced, so the average value of the lift is large and may reach an extreme value. When d/L -0.5, the leading-edge vortex is induced only by the forward vortex passing above the foil. Comparing to d/L 0, the leading-edge vortex is generated at a latter position. As the leading-edge vortex is generated only on one side of the foil, its strength is reduced. Both the thrust and lift on the foil are decreasing as well.

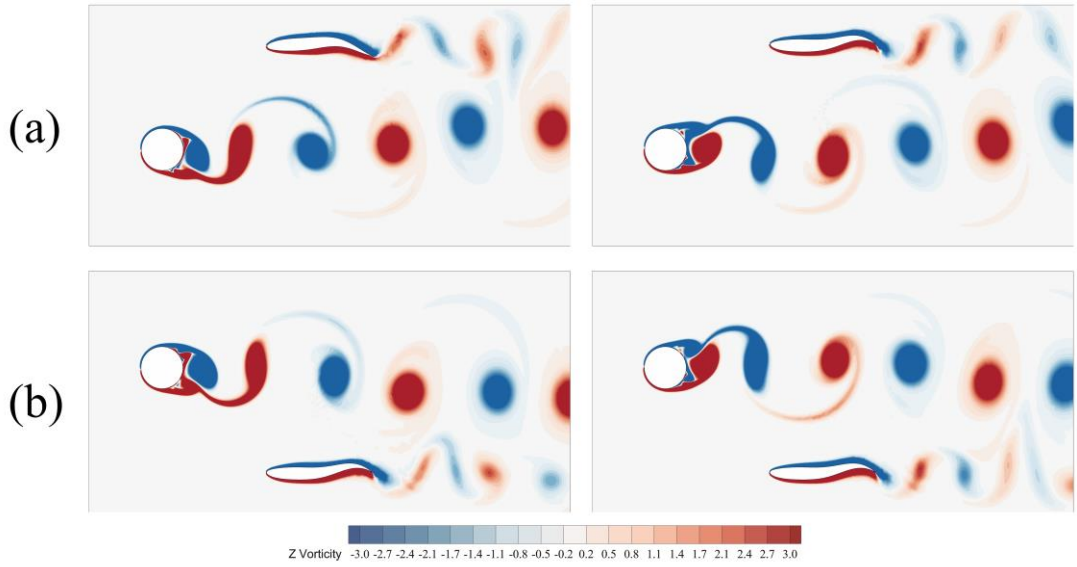

Figure 13 The vorticity contours of the undulating foil at (a) d/L 1 and (b) d/L -1.

When d/L -1 as shown in Figure 13, neither the positive vortex nor the negative vortex could cause the generation of the leading-edge vortex or secondary vortex. The Kármán vortex and the trailing vortex move side by side to the far field, and only a small trailing vortex is attracted by the Kármán vortex. Therefore, the lift and thrust of the undulating foil are relatively small. On the other hand, the undulating foil cannot be disturbed by the cylinder.

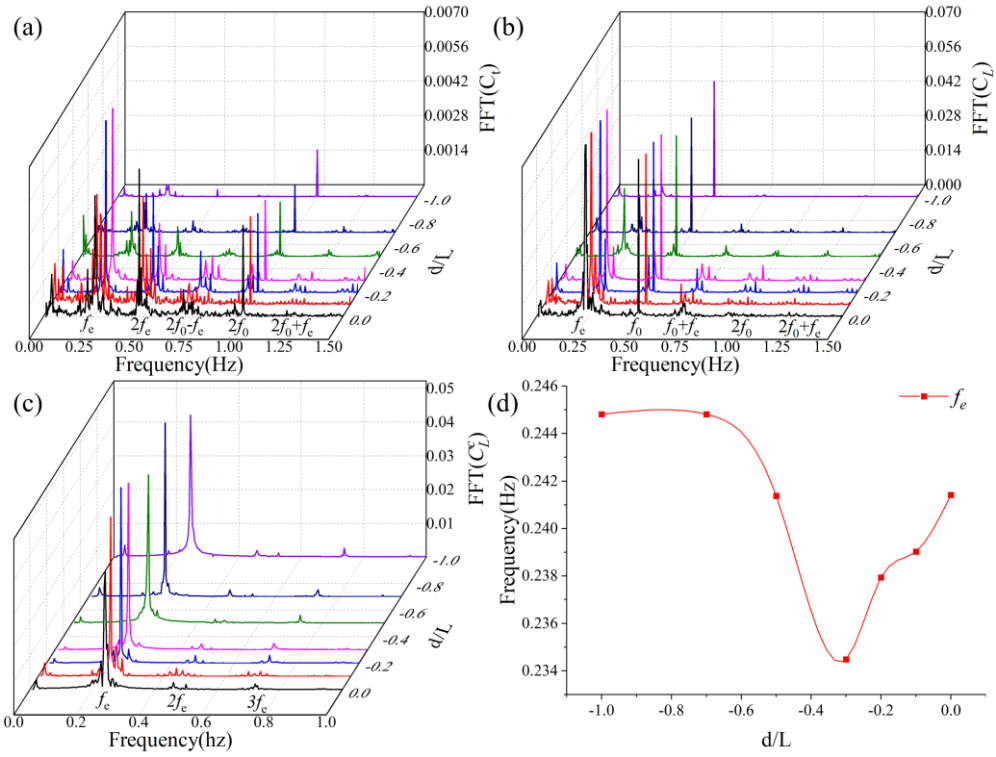

Figure 14 Fourier spectra of (a) C_t ,(b) C_L and(c) C_L^c acting on foil or cylinder and (d) shedding frequency f_e againt lateral distance.

Previous research[27] pointed out that the undulating foil reduces drag force of the cylinder by suppressing the shedding of the Kármán vortex street behind the cylinder. The results in Figure 14 confirm this conclusion. After performing FFT analysis on the force data of the foil and the cylinder, it was observed that the presence of the undulating foil reduces the shedding frequency of the cylinder. The spectral distribution of lift and drag for the foil includes the undulating frequency, shedding frequency of the cylinder, and their combination frequencies, as shown in Figure 14 (a) and (b). The presence of the shedding frequency of the cylinder as a single multiple in the combined frequencies reflects the direct impact of the Kármán vortex street on the foil. This finding is consistent with the results reported by Tong et al.[28]. Furthermore, the results indicate that the shedding frequency of the cylinder, obtained through FFT transformation of the force data, is dependent on the lateral distance. The lateral distance also influences the Fourier spectrum of the forces acting on the cylinder. As shown in Figure 14(c), it can be observed that the amplitude corresponding to the shedding frequency decreases as

the lateral distance decreases. Moreover, it is crucial to note that different lateral distances correspond to different shedding frequencies, as illustrated in Figure 14(d), where the shedding frequencies are extracted from Figure 14(c). The minimum frequency occurs at d/L -0.3, and the frequency at d/L 0 is smaller than that at d/L -1. This trend aligns with the evolution of the cylinder's drag. Based on the present results, it can be concluded that the range of optimal lateral distance is d/L ±0.3. Within this range, the drag reduction effect of the cylinder is optimal due to the suppression of the vortex shedding from the cylinder.

3.3. The Combined Effect of Lateral Distance and Longitudinal Distance

As previously discussed, the undulating foil positioned symmetrically relative to the cylinder's centreline exhibits similar kinematic performance. Therefore, this section focuses on the case where the undulating foil is located below the cylinder's centreline to explore its performance at various positions.

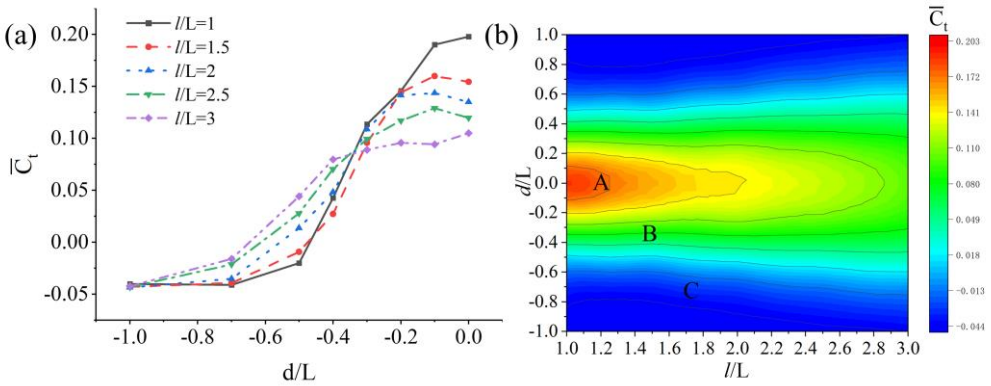

Figure 15(a)Variation curves of the average thrust coefficient of the undulating foil at different longitudinal distances with the lateral distance. (b)Thrust coefficient contours of the undulating foil at different lateral and longitudinal distances behind the cylinder.

According to Figure 15(a), the thrust coefficients of undulating foil with different longitudinal distances tend to increase with the decreasing lateral distance. When d/L is less than 0.2, a large longitudinal distance would lead to a small thrust coefficient. When d/L is close to 0.3, the thrust of the undulating foil is similar for all longitudinal

distances. When *d/L* is larger than 0.4, the larger the longitudinal distance, the smaller the thrust coefficient. When *d/L* is greater than 0.7, the thrust of the undulating foil at all longitudinal distances is consistent with that of the undulating foil in the UF case.

The thrust coefficient contour distribution is given in Figure 15(b). In order to better display the results, smoothing method has been adopted to display the contour map. The results show that there are three distinct regions distributed at different lateral and longitudinal distances. The high thrust zone A is distributed at low longitudinal distances and low lateral distances. The leading-edge vortex and secondary vortex are relatively strong in the high-thrust zone, and the undulating foil can absorb a large amount of energy to reduce its own movement costs. The middle thrust zone B is concentrated in the range of *d/L* 0.2-0.4, and as the longitudinal distance increases, the lateral distance corresponding to B becomes larger, which is also related to the range of action of the Kármán vortex street. The low thrust zone C is far away from the cylinder, and it is difficult for the undulating foil to utilize the energy of the Kármán vortex in the zone. In the reverse Kármán vortex street, whether the swimmer downstream can benefit from the vortex field often depends on the spacing and phase difference[41][43]. However, present research showed that with the selected *St* and *Re*, the downstream undulating foil in the Kármán vortex street is always able to extract energy from the vortex.

The lift performance of the undulating foil is shown in Figure 16. Regardless of the longitudinal distance, when *d/L* 0, the mean lift coefficient of the undulating foil is close to 0. The periodic effect of the Kármán vortex on the undulating foil is in kinetic equilibrium on its upper and lower surfaces. As the lateral distance increases, the absolute value of the mean lift coefficient tends to increase first and then decrease. The larger the longitudinal distance, the larger the lateral distance corresponding to the extreme value of lift. The high-lift zone partially overlaps with the middle thrust zone. In the high lift zone, the undulating foil is more unstable. From Figure 16, this range still occupies a large area.

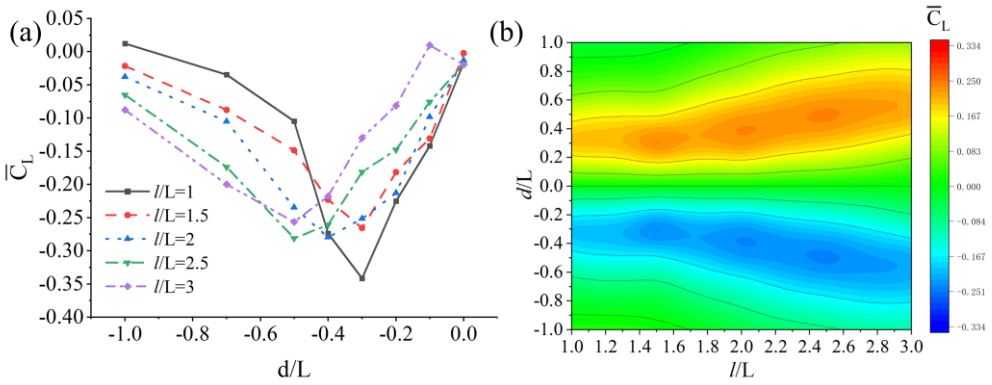

Figure 16 (a)Variation curves of the average lift coefficient of the undulating foil at different longitudinal distances with the lateral distance. (b)Lift coefficient contours of the undulating foil at different lateral and longitudinal distances behind the cylinder.

Figure 17 illustrates the contour of the average drag coefficient and lift coefficient of the cylinder. As shown in Figure 17(a), the area with the best drag reduction effect on the cylinder is primarily located at l/L 1.5 and the lateral distance is relatively small. A relatively large enhancement of lift is observed in the area of l/L 1 and d/L 0.3 for the undulating foil. The results show that the undulating foil has a greater influence on the cylinder only at a specific position. When the distance between the undulating foil and the cylinder is large, the influence of the undulating foil on the cylinder is negligible. The evolution of the vortex cannot reduce the drag of the cylinder, which shows that the phenomenon of the undulating foil reducing the vortex shedding frequency of the cylinder is limited by distance.

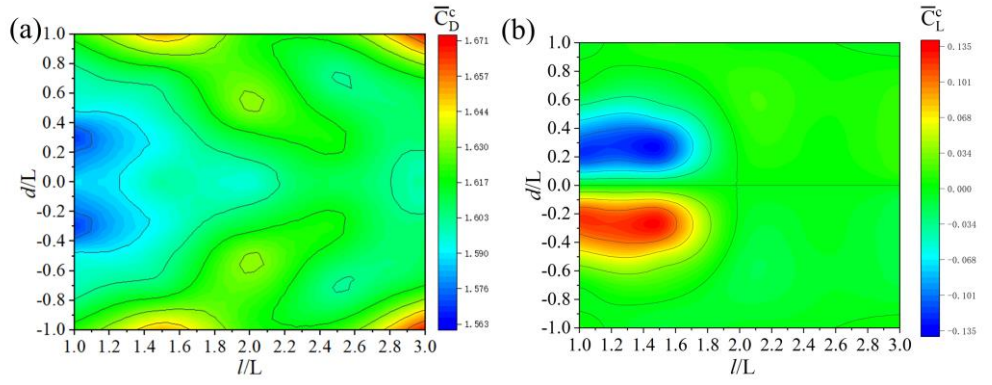

Figure 17 (a)Drag coefficient contours of the cylinder when the undulating foil is located at different lateral and longitudinal distances. (b)Lift coefficient contours of the cylinder when the undulating foil is located at different lateral and longitudinal distances.

The hydrodynamic performance of the undulating foil and its impact on the cylinder vary at different lateral and longitudinal distances. The role of the leading-edge vortex and secondary vortex in enhancing the thrust of the undulating foil is limited as the strength of these vortices varies in different locations, resulting in different thrusts generated by the undulating foil. With the selected *Re* and *St*, the thrust of the undulating foil increases and varies within the range of the Kármán vortex street radiation. The lateral distance of the radiation range has a certain limitation, and the mean lift is also related to the lateral distance. The increasing lift signifies the instability of the undulating foil. In summary, the hydrodynamic performance of the undulating foil shows different trends with the variation in longitudinal distance at different lateral distances. The leading-edge vortex and secondary vortex play a vital role in the process of enhancing the thrust of the undulating foil. These findings complement previous research.

4.Conclusions

In this study, numerical investigations are conducted to analyse the foil undulations downstream of a fixed cylinder at low Reynolds number. The hydrodynamic performance of cylinders and foils is thoroughly examined in conjunction with the evolution of vortices. The findings highlight the decisive role played by the evolution of the leading-edge vortex and secondary vortex in significantly improving the thrust performance of undulating foils. Numerical simulations are carried out under four distinct working conditions to discuss the mechanism behind the thrust enhancement of undulating foils in the Kármán vortex street. The results demonstrate that hydrofoils swimming in the Kármán vortex generate greater thrust compared to the combined thrust of foils in steady flow and stationary foils in the Kármán vortex. This can be attributed to the presence of leading-edge vortex and secondary vortex, which creates a substantial area of suction, including at the trailing edge of the undulating foil, thereby facilitating thrust generation.

The study further investigates the behaviour of undulating foils at different lateral distances swimming in the Kármán vortex street, observing variations in the evolution of the leading-edge vortex and the secondary vortex. The results reveal that increasing the lateral distance weakens the main vortex, which in turn affects the generation of the secondary vortex and hampers thrust improvement. The thrust of the corrugated hydrofoil decreases with increasing lateral distance, while the lift initially increases and then decreases. Additionally, the shedding frequency of the cylinder varies with the lateral distance, determining the change in resistance trend. Moreover, the combined impact of both lateral and longitudinal distances on undulated foils and cylinders is found to be significant. To be summarised, the key finding could be as following:

1. The foil with undulating motion can obtain energy more easily in the Kármán vortex street.
2. Both leading-edge and secondary vortex can influence either thrust enhancement or lift of the foil.
3. The combined influence of lateral and longitudinal distances on an undulated foil is explored for the first time.
4. Unlike in the reverse Kármán vortex street, the undulating foil always achieves an enhanced thrust effect in the Kármán vortex street. However, the undulating foil has a distance limitation to decrease the vortex shedding frequency of a cylinder.

The insights in vortex dynamics of fish swimming downstream of blunt objects can significantly advance the designs of bionic fish robots in the direction of intelligent perception and maximum efficiency. Implementing suitable vortex management techniques can notably boost the propulsion capabilities of bionic fish robots. The cases in this study are under specified *St* and *Re* numbers and are limited to two-dimensional research. Future work could be expanded to three dimensions or employ flow field visualisation methods[44][45] to further investigate the vortices and explain the reason for fish thrust enhancement in unsteady flow.

Acknowledgements

This work was supported by the National Natural Science Foundation of China (No. 52301366). Results were obtained using ARCHIE-WeSt High Performance Computer (www.archie-west.ac.uk) based at the University of Strathclyde.

Data Availability Statement

The data that support the findings of this study are available within the article.

Reference

[1] Gao, P., Huang, Q., Pan, G., Ma, Y., & Song, D. (2022). Research on the hydrodynamic performance of double manta ray gliding in groups with variable attack angles. Physics of Fluids, 34(11),111908.

[2] Akanyeti, O., Putney, J., Yanagitsuru, Y. R., Lauder, G. V., Stewart, W. J., & Liao, J. C. (2017). Accelerating fishes increase propulsive efficiency by modulating vortex ring geometry. Proceedings of the National Academy of Sciences, 114(52), 13828-13833.

[3] Fish, F. E. (2006). The myth and reality of Gray's paradox: implication of dolphin drag reduction for technology. Bioinspiration & Biomimetics, 1(2), R17.

[4] Lewin, G. C., & Haj-Hariri, H. (2003). Modelling thrust generation of a two-dimensional heaving airfoil in a viscous flow. Journal of Fluid Mechanics, 492, 339-362.

[5] Borazjani, I., & Sotiropoulos, F. (2008). Numerical investigation of the hydrodynamics of carangiform swimming in the transitional and inertial flow regimes. Journal of Experimental Biology, 211(10), 1541-1558.

[6] Ashraf, M. A., Young, J., & Lai, J. C. S. (2011). Reynolds number, thickness and camber effects on flapping airfoil propulsion. Journal of Fluids and Structures, 27(2), 145-160.

[7] Thekkethil, N., Sharma, A., & Agrawal, A. (2020). Self-propulsion of fishes-like undulating hydrofoil: A unified kinematics based unsteady hydrodynamics study. Journal of Fluids and Structures, 93, 102875.

[8] Yu, Y. L., & Huang, K. J. (2021). Scaling law of fish undulatory propulsion. Physics of Fluids, 33(6), 061905.

[9] Chao, L. M., Alam, M. M., & Cheng, L. (2022). Hydrodynamic performance of slender swimmer: effect of travelling wavelength. Journal of Fluid Mechanics, 947, A8.

[10] Gupta, S., Sharma, A., Agrawal, A., Thompson, M. C., & Hourigan, K. (2021). Hydrodynamics of a fish-like body undulation mechanism: Scaling laws and regimes for vortex wake modes. Physics of Fluids, 33(10).

[11] Neogi, I., Niral Shah, V., Dev Singh, P., & Joshi, V. (2023). Propulsion of a combined heaving and trailing-edge morphing foil for bio-inspired applications. Physics of Fluids, 35(4),101904.

[12] Huang, S., Guo, D., Wang, Y., Yang, G., & Yin, B. (2023). Hydrodynamics of morphology for thunniform swimmers: Effects of the posterior body shape. Ocean Engineering, 272, 113866.

[13] Kang, L., Peng, Z. R., Huang, H., Lu, X. Y., & Cui, W. (2021). Active external control effect on the collective locomotion of two tandem self-propelled flapping plates. Physics of Fluids, 33(10),101901.

[14] Ren, K., Yu, J., Li, H., & Feng, H. (2022). Numerical investigation on the swimming mode and stable spacing with two self-propelled fish arranged in tandem. Ocean Engineering, 259, 111861.

[15] Wei, C., Hu, Q., Zhang, T., & Zeng, Y. (2022). Passive hydrodynamic interactions in minimal fish schools. Ocean Engineering, 247, 110574.

[16] Yu, H., Lu, X. Y., & Huang, H. (2021). Collective locomotion of two uncoordinated undulatory self-propelled foils. Physics of Fluids, 33(1),011904.

[17] Ma, Q., Ding, L., & Huang, D. (2021). A study on the influence of schooling patterns on the energy harvest of double undulatory airfoils. Renewable Energy, 174, 674-687.

[18] Maertens, A. P., Gao, A., & Triantafyllou, M. S. (2017). Optimal undulatory swimming for a single fish-like body and for a pair of interacting swimmers. Journal of Fluid Mechanics, 813, 301-345.

[19] Gopalkrishnan, R., Triantafyllou, M. S., Triantafyllou, G. S., & Barrett, D. (1994). Active vorticity control in a shear flow using a flapping foil. Journal of Fluid Mechanics, 274, 1-21.

[20] Liao, J. C., Beal, D. N., Lauder, G. V., & Triantafyllou, M. S. (2003). The Kármán gait: novel body kinematics of rainbow trout swimming in a vortex. Journal of Experimental Biology, 206(6), 1059-1073.

[21] Liao, J. C., Beal, D. N., Lauder, G. V., & Triantafyllou, M. S. (2003). Fish exploiting vortices decrease muscle activity. Science, 302(5650), 1566-1569.

[22] Beal, D. N., Hover, F. S., Triantafyllou, M. S., Liao, J. C., & Lauder, G. V. (2006). Passive propulsion in vortex wakes. Journal of Fluid Mechanics, 549, 385-402.

[23] Harvey, S. T., Muhawenimana, V., Müller, S., Wilson, C. A., & Denissenko, P. (2022). An inertial mechanism behind dynamic station holding by fish swinging in a vortex street. Scientific Reports, 12(1), 12660.

[24] Liao, Q., Dong, G. J., & Lu, X. Y. (2004). Vortex formation and force characteristics of a foil in the wake of a circular cylinder. Journal of Fluids and Structures, 19(4), 491-510.

[25] Eldredge, J. D., & Pisani, D. (2008). Passive locomotion of a simple articulated fish-like system in the wake of an obstacle. Journal of Fluid Mechanics, 607, 279-288.

[26] Alben, S. (2010). Passive and active bodies in vortex-street wakes. Journal of Fluid Mechanics, 642, 95-125.

[27] Xiao, Q., Sun, K., Liu, H., & Hu, J. (2011). Computational study on near wake interaction between undulation body and a D-section cylinder. Ocean Engineering, 38(4), 673-683.

[28] Tong, Y., Xia, J., & Chen, L. (2021). Study on energy extraction of Kármán gait hydrofoils from passing vortices. Physics of Fluids, 33(12), 121906.

[29] Shao, X., Pan, D., Deng, J., & Yu, Z. (2010). Hydrodynamic performance of a fishlike undulating foil in the wake of a cylinder. Physics of Fluids, 22(11), 111903.

[30] Khalid, M. S. U., Akhtar, I., & Dong, H. (2016). Hydrodynamics of a tandem fish school with asynchronous undulation of individuals. Journal of Fluids and Structures, 66, 19-35.

[31] Wei, C., Hu, Q., Liu, Y., Yin, S., Chen, Z., & Ji, X. (2021). Performance evaluation and optimization for two-dimensional fish-like propulsion. Ocean Engineering, 233, 109191.

[32] Zhao, C., Zhang, T., Yang, Y., & Dong, H. (2022). Sound generated by flow over two traveling wavy foils in a side-by-side arrangement. Physics of Fluids, 34(12),127120.

[33] Zhu, Y., Tian, F. B., Young, J., Liao, J. C., & Lai, J. C. (2021). A numerical study of fish adaption behaviours in complex environments with a deep reinforcement learning and immersed boundary–lattice Boltzmann method. Scientific Reports, 11(1), 1691.

[34] Sun, P. N., Colagrossi, A., & Zhang, A. M. (2018). Numerical simulation of the self-propulsive motion of a fishlike swimming foil using the δ+-SPH model. Theoretical and Applied Mechanics Letters, 8(2), 115-125.

[35] Rahmat, A., Nasiri, H., Goodarzi, M., & Heidaryan, E. (2020). Numerical investigation of anguilliform locomotion by the SPH method. International Journal of Numerical Methods for Heat & Fluid Flow, 30(1), 328-346.

[36] Dong, G. J., & Lu, X. Y. (2007). Characteristics of flow over traveling wavy foils in a side-by-side arrangement. Physics of Fluids, 19(5),057107.

[37] Li, Z. Y., Feng, L. H., Kissing, J., Tropea, C., & Wang, J. J. (2020). Experimental investigation on the leading-edge vortex formation and detachment mechanism of a pitching and plunging plate. Journal of Fluid Mechanics, 901, A17.

[38] Verma, S., Novati, G., & Koumoutsakos, P. (2018). Efficient collective swimming by harnessing vortices through deep reinforcement learning. Proceedings of the National Academy of Sciences, 115(23), 5849-5854.

[39] Novati, G., Verma, S., Alexeev, D., Rossinelli, D., Van Rees, W. M., & Koumoutsakos, P. (2017). Synchronisation through learning for two self-propelled swimmers. Bioinspiration & Biomimetics, 12(3), 036001.

[40] Seo, J. H., & Mittal, R. (2022). Improved swimming performance in schooling fish via leading-edge vortex enhancement. Bioinspiration & Biomimetics, 17(6), 066020.

[41] Joshi, V., & Mysa, R. C. (2021). Mechanism of wake-induced flow dynamics in tandem flapping foils: Effect of the chord and gap ratios on propulsion. Physics of Fluids, 33(8), 087104.

[42] Muscutt, L. E., Weymouth, G. D., & Ganapathisubramani, B. (2017). Performance augmentation mechanism of in-line tandem flapping foils. Journal of Fluid Mechanics, 827, 484-505.

[43] Broering, T. M., Lian, Y., & Henshaw, W. (2012). Numerical investigation of energy extraction in a tandem flapping wing configuration. AIAA journal, 50(11), 2295-2307.

[44] Guo, C. Y., Kuai, Y. F., Han, Y., Xu, P., Fan, Y. W., & Yu, C. D. (2022). Hydrodynamic analysis of propulsion process of zebrafish. Physics of Fluids, 34(2), 021910

[45] Guo, C. Y., Liang, Z. J., Han, Y., Xu, P., Wang, Y. H., & Kuai, Y. F. (2022). Hydrodynamic mechanism of Misgurnus anguillicaudatus during turning maneuvers. Physics of Fluids, 34(9), 095130.